ISSN 0030-400X, Optics and Spectroscopy, 2012, Vol. 112, No. 4, pp. 585–593. © Pleiades Publishing, Ltd., 2012.
Original Russian Text © S.Ya. Vetrov, N.V. Rudakova, I.V. Timofeev, V.P. Timofeev, 2012, published in Optika i Spektroskopiya, 2012, Vol. 112, No. 4, pp. 638–646.

CONDENSED-MATTER SPECTROSCOPY

Spectral Properties of a Two-Dimensional Resonant Metal–Dielectric Photonic Crystal

S. Ya. Vetrov[a], N. V. Rudakova[a], I. V. Timofeev[b], and V. P. Timofeev[a]

[a] *Siberian Federal University, Krasnoyarsk, 660074 Russia*

[b] *Kirensky Institute of Physics, Siberian Branch, Russian Academy of Sciences, Akademgorodok, Krasnoyarsk, 660036 Russia*

e-mail: atrum528@mail.ru; tiv@iph.krasn.ru

Received July 25, 2011; in final form, October 19, 2011

Abstract—We have studied the transmission spectra of resonant two-dimensional photonic crystals of two types, one of which consists of nanocomposite cylinders that form a square lattice in vacuum and the other of which consists of cylindrical holes that form a square lattice in nanocomposite matrix. The nanocomposite consists of metallic nanospheres that are dispersed in a transparent matrix and is characterized by an effective resonant dielectric permittivity. We show that, depending on the position of the resonant frequency of the nanocomposite with respect to the boundaries of the band gap, there arises either an additional transmission band in the transmission spectrum in the band gap or an additional band gap in the continuous spectrum of the photonic crystal. As the structural and geometric parameters of the system change, both the additional transmission band and the additional band gap are considerably modified. We analyze particular features of the spatial distribution of the electromagnetic field intensity in crystals. The considered effects can be used to extend the possibilities of creating new photonic crystals with specified properties.

DOI: 10.1134/S0030400X12030204

INTRODUCTION

At present, a constantly increasing number of basic and applied investigations have been devoted to the development of fundamental foundations of branches that are alternatives to semiconductor electronics. The main goal of photonics is to create information transmission and processing facilities in which photons, rather than electrons, would be the basic carriers. To create optical integral schemes, "optical semiconductors," i.e., materials that have photonic band gaps in their intrinsic energy spectra and that were termed the photonic crystals are also necessary. This is a new class of materials for optoelectronics and nanophotonics, which are attracting interest as new optical materials with unique properties [1–4]. The occurrence of photonic band gaps makes it possible to control spontaneous emission; these gaps lead to light localization effects and open the way for applications of photonic crystals in laser engineering, quantum computers, and systems of optical communication and information transmission. Photonic crystals with tunable spectral characteristics are of considerable interest. The spectral properties of a photonic crystal can be significantly changed by placing resonant media into its periodic structure. However, these changes manifest themselves only in a narrow frequency range near the resonant frequency; therefore, this photonic crystal is termed the resonant photonic crystal. The combination of the dispersion of a resonant medium with an intrinsic dispersion of a photonic crystal opens up new opportunities for controlling the spectral and optical properties of photonic crystals. In [5, 6], particular features of the band structure and of the transmission spectrum of two-dimensional (2D) resonant photonic crystals in which a resonant gas serves as one of the composite materials were studied. Composite media with metal nanoparticles are of great interest in connection with the creation of nanostructured metal–dielectric photonic crystals and devising new methods of light control on their basis [7, 8]. For a nanocomposite that consists of metallic nanoparticles suspended in a transparent matrix, the occurrence of a resonance of an effective dielectric permittivity has been predicted [9, 10]; at the same time, the optical characteristics of the initial materials do not show any resonant properties. The position of the resonance, which lies in the visible light range, depends on the dielectric permittivities of the initial materials and the concentration and shape of nanoparticles.

In this work, using a modified transfer-matrix method [11, 12], which follows from the finite difference method in the time domain [13, 14], we study the transmission spectra of 2D resonant photonic crystals of the following two types: (i) elements of the crystal of the first type are nanocomposite cylinders that form a square lattice in vacuum, and (ii) elements of the crystal of the second type are cylindrical holes that form a square lattice in a nanocomposite matrix. The nanocomposite consists of metallic nanoparticles that are

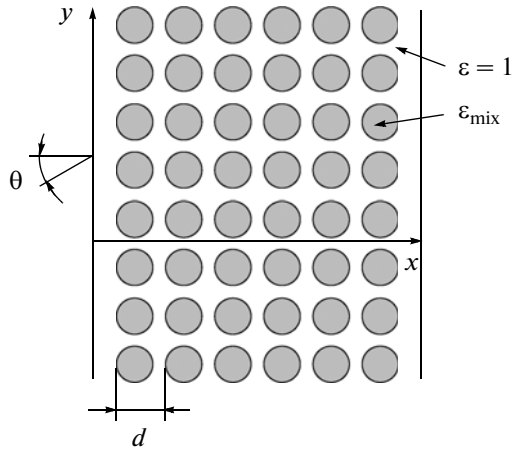

Fig. 1. Scheme of the layer of the structure of a two-dimensional photonic crystal of the first type that is composed of six rows of nanocomposite cylinders with a dielectric permittivity ε_{mix} that form a square lattice in vacuum; d is the lattice period, θ is the angle of incidence (top view).

dispersed in a transparent matrix and is characterized by the effective resonant dielectric permittivity $\varepsilon_{mix}(\omega)$.

PHYSICAL MODEL OF A PHOTONIC CRYSTAL

Consider, as in [6], a resonant photonic crystal in a shape of a plate that is infinite in two directions, has a finite thickness, and is in vacuum. We will assume that the axes of cylinders are perpendicular to the *xy* plane and are parallel to the *z* axis and the centers of the cross sections of cylinders form a square lattice in the *xy* plane. Waves with an *s* polarization propagate in the *xy* plane along the *x* axis. For the resonant photonic crystal of the first type, the nanocomposite cylinders that form its crystalline structure consist of spherical silver nanoparticles randomly distributed in a transparent dielectric matrix (Fig. 1). The resonant photonic crystal of the second type consists of infinite cylindrical holes that form a square lattice in a nanocomposite matrix.

The dielectric permittivity ε_{mix} is defined by the Maxwell-Garnett formula, which is widely used in studies of matrix media that contain dispersed inclusions of a small volume fraction [9, 10, 15, 16],

$$\varepsilon_{mix} = \varepsilon_d\left[1+\frac{f}{(1-f)/3+\varepsilon_d/(\varepsilon_m-\varepsilon_d)}\right], \qquad (1)$$

where f is the filling factor, i.e., the fraction of nanoparticles in the matrix; $\varepsilon_m(\omega)$ and ε_d are the dielectric permittivities of the metal of which nanoparticles are made and of the matrix, respectively; and ω is the radiation frequency. The size of nanoparticles is much smaller than the wavelength and the penetration depth of the field into the material. The dielectric permittivity of the metal of nanoparticles can be found using the Drude approximation,

$$\varepsilon_m(\omega) = \varepsilon_0 - \frac{\omega_p^2}{\omega(\omega+i\gamma)}, \qquad (2)$$

where ε_0 is the constant that takes into account the contributions from interband transitions of coupled electrons, ω_p is the plasma frequency, and γ is the quantity that is the inverse of the electron relaxation time.

The function $\varepsilon_{mix}(\omega)$ is complex,

$$\varepsilon_{mix}(\omega) = \varepsilon'_{mix}(\omega) + i\varepsilon''_{mix}(\omega).$$

By neglecting the small factor γ^2, we find the position of the resonant frequency, which depends on the characteristics of initial materials and concentration f of the disperse phase,

$$\omega_0 = \omega_p\sqrt{\frac{1-f}{3\varepsilon_d+(1-f)(\varepsilon_0-\varepsilon_d)}}. \qquad (3)$$

At the point $\omega = \omega_0$, the function $\varepsilon'_{mix}(\omega)$ turns to zero and $\varepsilon''_{mix}(\omega)$ acquires a maximal value. The function $\varepsilon'_{mix}(\omega)$ also turns to zero at the point

$$\omega_1 = \omega_p\sqrt{\frac{1+2f}{(\varepsilon_0+2\varepsilon_d+2f(\varepsilon_0-\varepsilon_d))}}. \qquad (4)$$

In the interval $[\omega_0, \omega_1]$, the function $\varepsilon'_{mix}(\omega) < 0$; i.e., in this frequency range, the nanocomposite is similar to a metal.

METHOD OF CALCULATION OF THE SPECTRUM AND FIELD IN THE MEDIUM

To calculate the transmission spectrum of *s* polarized electromagnetic waves that propagate in the *xy* plane and the electric vector of which is parallel to the *z* axis, we used the formalism of the transfer-matrix method, which was developed for one-dimensional layered media and then was expanded to two- and three-dimensional photonic crystals. The transfer-matrix relates the amplitudes of plane waves at the exit from the medium with amplitudes of waves at the entrance to the medium. This matrix is formed by multiplication of matrices that relate the amplitudes of plane waves in adjacent thin layers into which the sample is separated. However, in a photonic crystal with a dimensionality higher than the first, the transfer-matrix is unstable and exponentially diverges because its eigenvalues increase according to a geometric progression law with increasing number of layers. To eliminate this peculiarity, the transfer-matrix is transformed into scattering matrix, which makes it possible

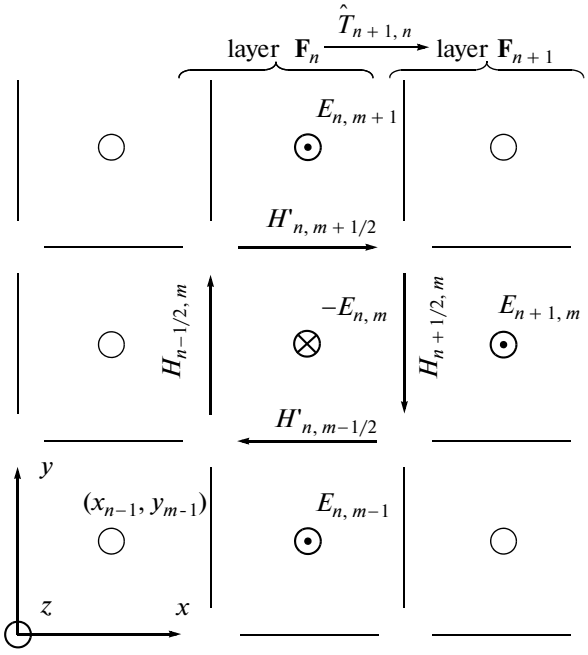

Fig. 2. Numerical grid. Circles denote lines along the z axis, which is perpendicular to the plane of the figure. The lines of the strength that are involved in formulas of (7)–(10) of transfer to the adjacent layer are shown in bold.

to eliminate numerical instabilities and calculate the transmission coefficients.

To construct the transfer-matrix, we will use two Maxwell electrodynamic equations written in the integral form in the Gaussian CGS units. These are the Faraday induction law,

$$-\frac{1}{c}\frac{d}{dt}\int_s \mathbf{B}d\mathbf{s} = \oint_l \mathbf{E}d\mathbf{l} \tag{5}$$

and the Ampere circulation theorem, which was generalized by Maxwell with allowance for the displacement current,

$$\frac{4\pi}{c}I + \frac{1}{c}\frac{d}{dt}\int_s \mathbf{D}d\mathbf{s} = \oint_l \mathbf{H}d\mathbf{l}. \tag{6}$$

Here, **B** and **D** are the magnetic and electric induction vectors, respectively; **H** and **E** are the vectors of the magnetic and electric field strengths, respectively; the contour l is the boundary of the surface S; and I is the current that, in this problem, is zero.

As an integration contour, we will choose cells of a numerical grid (Fig. 2) [11, 13, 14]. A half-integer index of the magnetic field means that nodes of the magnetic field are located precisely in the middle between nodes for the electric field. The electric contour for the Faraday law (5) consists of the lines of the strengths $E_{n,m}$ and $E_{n,m+1}$ that emerge from the plane of the figure and are directed along the z axis,

$$-idH'_{n,m+1/2} = E_{n,m+1} - E_{n,m}. \tag{7}$$

Here, H' is the cell-averaged amplitude of the x component of the magnetic field; $d = (y_{m+1} - y_m)\omega/c$ is the dimensionless increment of the phase that was obtained as a result of differentiating the stationary magnetic field $H_x = H'\exp(i\omega t)$ with respect to time. Similarly, the other two electric contours yield

$$-idH'_{n,m-1/2} = E_{n,m} - E_{n,m-1}, \tag{8}$$

$$idH_{n+1/2,m} = E_{n+1,m} - E_{n,m}, \tag{9}$$

where H is the cell-averaged amplitude of the y component of the magnetic field. For simplicity, we use the square grid $y_{m+1} - y_m = x_{n+1} - x_n$.

The magnetic contour for Ampere theorem (6) is a square cell of the grid lying in the plane of the figure,

$$id\varepsilon E_{n,m} = H_{n-1/2,m} - H'_{n+1/2,m} + H'_{n,m+1/2} - H'_{n,m-1/2}. \tag{10}$$

Here, ε is the complex dielectric permittivity of an optical medium in the cell including the absorption via the imaginary part. It is assumed that the medium within the cell is homogeneous.

H' is eliminated from system (7)–(10),

$$\begin{aligned} H_{n+1/2,m} &= H_{n-1/2,m} - id\varepsilon E_{n,m} + H'_{n,m+1/2} - H'_{n,m-1/2} \\ &= H_{n-1/2,m} - id\varepsilon E_{n,m} - \frac{i}{d}\left(2E_{n,m} - E_{n,m-1} - E_{n,m+1}\right), \end{aligned} \tag{11}$$

$$\begin{aligned} E_{n+1,m} &= E_{n,m} + idH_{n+1/2,m} \\ &= idH_{n-1/2,m} + d^2\varepsilon E_{n,m} + \left(3E_{n,m} - E_{n,m-1} - E_{n,m+1}\right). \end{aligned} \tag{12}$$

In matrix form, this is written as

$$\begin{bmatrix} \begin{bmatrix} E_{n+1,1} \\ \vdots \\ E_{n+1,M} \end{bmatrix} \\ \begin{bmatrix} H_{n+1/2,1} \\ \vdots \\ H_{n+1/2,M} \end{bmatrix} \end{bmatrix} = \begin{bmatrix} \begin{bmatrix} (3-d^2\varepsilon) & -1 & 0 \\ -1 & \ddots & \ddots \\ 0 & \ddots & \ddots \end{bmatrix} \begin{bmatrix} id & & 0 \\ & \ddots & \\ 0 & & id \end{bmatrix} \\ \begin{bmatrix} i(d\varepsilon - 2/d) & id & 0 \\ id & \ddots & \ddots \\ 0 & \ddots & \ddots \end{bmatrix} \begin{bmatrix} 1 & & 0 \\ & \ddots & \\ 0 & & 1 \end{bmatrix} \end{bmatrix} \cdot \begin{bmatrix} \begin{bmatrix} E_{n,1} \\ \vdots \\ E_{n,M} \end{bmatrix} \\ \begin{bmatrix} H_{n-1/2,1} \\ \vdots \\ H_{n-1/2,M} \end{bmatrix} \end{bmatrix}. \tag{13}$$

Here, the zeros denote the triangle blocks of the matrices the elements of which are zeros. By denoting the field in the layer of the medium as **F** the transfer-matrix as $\hat{T}$, we can write (13) in the compact form

$$\mathbf{F}_{n+1} = \hat{T}_{n+1,n}\mathbf{F}_n, \quad \mathbf{F} = \begin{bmatrix}\mathbf{E}\\ \mathbf{H}\end{bmatrix}. \tag{14}$$

The vector of the field **F** consists of two blocks, which determine the electric $\mathbf{E} = [E_m]$ and magnetic $\mathbf{H} = [H_m]$ components. The dimension of the block M is equal to the number of nodes in the layer of the computational grid. The transfer-matrix is formed by combining four square matrices with a dimension of $M \times M$.

The field in the node of the grid can be represented as a superposition of plane waves,

$$E_z(x,y) = \sum_q A_q \exp(-ik_{q,x}x - ik_{q,y}y) + B_q \exp(+ik_{q,x}x - ik_{q,y}y), \tag{15}$$

$$H_y(x,y) = \sum_q -\frac{k_{q,x}}{k} A_q \exp(-ik_{q,x}x - ik_{q,y}y) + \frac{k_{q,x}}{k} B_q \exp(+ik_{q,x}x - ik_{q,y}y). \tag{16}$$

Here, A_q and B_q are the amplitudes of waves that are incident onto layer of the grid from the left and from the right. The set of wavenumbers $k = \sqrt{\varepsilon}\omega/c$ corresponds to the wavenumber $\mathbf{k}_q = (k_{q,x}, k_{q,y})$. The y component of the wave vector $k_{q,y}$, which is tangential to the layer of the grid, is preserved upon passage from layer to layer. In accordance with the Bloch theorem, $k_{q,y} = k_{0y} + 2\pi q/d$, where q is the integer between $-M/2$ and $M/2$ (for even M), d is the lattice period of the photonic crystal, and $\mathbf{k}_0$ is the wave vector of the incident wave. Equations (15) and (16) can also be written in the matrix form

$$\mathbf{F}_n = \hat{R}_n\mathbf{W}_n, \quad \mathbf{F} = \begin{bmatrix}\mathbf{E}\\ \mathbf{H}\end{bmatrix}, \quad \mathbf{W} = \begin{bmatrix}\mathbf{A}\\ \mathbf{B}\end{bmatrix},$$

where $\hat{R}$ is the field transformation matrix and **W** is the vector of the amplitudes of plane waves, which consists of blocks $\mathbf{A} = [A_q]$ and $\mathbf{B} = [B_q]$. The transfer-matrix $\hat{T}_{n+1,n}$ can also be transformed to the wave representation $\hat{\tilde{T}}_{n+1,n}$,

$$\mathbf{W}_{n+1} = \hat{R}_{n+1}^{-1}\mathbf{F}_{n+1} = \hat{R}_{n+1}^{-1}\hat{T}_{n+1,n}\mathbf{F}_n = \hat{R}_{n+1}^{-1}\hat{T}_{n+1,n}\hat{R}_n\mathbf{W}_n = \hat{\tilde{T}}_{n+1,n}\mathbf{W}_n. \tag{17}$$

Transfer-matrix (13) contains a numerical instability. The eigenvalues of this matrix exceed unity and increase according to a geometric progression law as matrices of adjacent layers are multiplied. The transfer-matrix of the one-dimensional problem can also diverge in the case of the total internal reflection if a surface wave with an imaginary wave vector transverse to layers appears. In the two-dimensional problem, these surface waves should be taken into account in any case. The described instability occurs due to the violation of the cause-and-effect relation. The waves $\mathbf{B}_{n+1}$ that are incident on the layer are defined via the waves $\mathbf{B}_n$ that are reflected from the layer and that are a consequence of the interaction of the light with the layer,

$$\begin{bmatrix}\mathbf{A}_{n+1}\\ \mathbf{B}_{n+1}\end{bmatrix} = \hat{\tilde{T}}_{n+1,n}\begin{bmatrix}\mathbf{A}_n\\ \mathbf{B}_n\end{bmatrix}, \hat{\tilde{T}}_{n+1,n} = \begin{bmatrix}\hat{a} & \hat{b}\\ \hat{c} & \hat{d}\end{bmatrix}. \tag{18}$$

Equation (18) can also be described as

$$\begin{bmatrix}\mathbf{B}_n\\ \mathbf{A}_{n+1}\end{bmatrix} = \hat{S}_{n+1,n}\begin{bmatrix}\mathbf{A}_n\\ \mathbf{B}_{n+1}\end{bmatrix}, \quad \hat{S}_{n+1,n} = \begin{bmatrix}\hat{r}_+ & \hat{t}_+\\ \hat{t}_- & \hat{r}_-\end{bmatrix} = \begin{bmatrix}-\hat{d}^{-1}\hat{c} & \hat{d}^{-1}\\ \hat{a} - \hat{b}\hat{d}^{-1}\hat{c} & \hat{b}\hat{d}^{-1}\end{bmatrix}. \tag{19}$$

Therefore, the formalism of the light scattering by the layer restores the physical meaning with the aid of the scattering matrix $\hat{S}_{n+1,n}$, which consists of complex transmission $\hat{t}_\pm = [t_{qq'}^\pm]$ and reflection $\hat{r}_\pm = [r_{qq'}^\pm]$ amplitude coefficients. Each of these coefficients does not exceed unity in magnitude, which prevents the divergence.

However, the numerical difficulty of combining matrices for adjacent layers is the price one has to pay for the stability of the scattering matrix. For transfer-matrices, it suffices to perform the matrix multiplication $\hat{T}_{n+2,n} = \hat{T}_{n+2,n+1}\hat{T}_{n+1,n}$, which, for sparse matrices, requires about $O(M)$ operations. For scattering matrices (Fig. 3), the formula of multiple scattering [12] is used

$$\hat{S}_{n+2,n} = \begin{bmatrix}\hat{r}_+ + \hat{t}_-(\hat{1} - \hat{r}'_+\hat{r}_-)^{-1}\hat{r}'_+\hat{t}_+ & \hat{t}'_+(\hat{1} - \hat{r}_-\hat{r}'_+)^{-1}\hat{t}_+\\ \hat{t}_-(\hat{1} - \hat{r}'_+\hat{r}_-)^{-1}\hat{t}'_- & \hat{t}'_- + \hat{t}'_+(\hat{1} - \hat{r}_-\hat{t}'_+)^{-1}\hat{r}_-\hat{t}'_-\end{bmatrix}, \tag{20}$$

where $\hat{1}$ is the $M \times M$ unit matrix and the primes denote the four blocks of the matrix $\hat{S}_{n+2,n+1}$. This calculation requires about $O(M^3)$ elementary operations. Therefore, a significant advantage in calculations is obtained if nonsingular transfer-matrices of individual layers in a thin stack are initially combined and then the scattering matrices of adjacent stacks are combined.

As a result of combining, the matrix $\hat{S}_{N,1}$ yields explicit transmission and reflection spectra of all the

N layers. The energy transmission and reflection coefficients T and R are given by

$$T = \sqrt{\frac{\varepsilon_N}{\varepsilon_1}}\sum_q \left|t^2_{+q0}\right| \mathrm{Re}(k_{Nqx})/k_{0x},$$
$$R = \sum_q \left|r^2_{+q0}\right| \mathrm{Re}(k_{1qx})/k_{0x}, \quad (21)$$

where t_{+q0}, r_{+q0} are elements of the middle column for the matrices $\hat{t}_+$ and $\hat{r}_+$, which correspond to the amplitudes of scattered waves. The ratio k_x/k_{0x} is responsible for the area through which an oblique ray is incident onto the layer. Surface waves are not involved in the energy transfer transverse to layers.

To calculate the field in a medium, one has to impose the boundary condition at the entrance of the medium. The field at the left boundary of the medium is

$$\mathbf{W}_1 = \begin{bmatrix} A_1 \\ B_1 \end{bmatrix}.$$

The amplitudes of reflected waves $B_{1q} = r_{+q0}$ are determined from the matrix $\hat{S}_{N,1}$. The vector of waves that are incident from the left will contain only one nonzero element $A_{10} = 1$, which corresponds to a plane input unit wave. From the field at the boundary, one can easily obtain amplitudes of waves $\mathbf{W}$ and of field strengths $\mathbf{F}$ and local intensity I of the field in the nth layer,

$$\mathbf{W}_n = \hat{\hat{T}}_{n,1}\mathbf{W}_1, \quad \begin{bmatrix} \mathbf{E}_n \\ \mathbf{H}_n \end{bmatrix} = \mathbf{F}_n = \hat{R}_n\mathbf{W}_n,$$
$$I(x_n, y_m) = \left|E_{n,m}\right|^2. \quad (22)$$

To this end, it is necessary to store partial scattering matrices $\hat{S}_{2,1}$, $\hat{S}_{3,1}$, ..., $\hat{S}_{N,1}$ or transfer-matrices $\hat{\hat{T}}_{2,1}$, $\hat{\hat{T}}_{3,1}$, ..., $\hat{\hat{T}}_{N,1}$ in computer memory. However, in practice, it is convenient to calculate these matrices again.

CALCULATION RESULTS AND THEIR DISCUSSION

First of all, we consider the results of calculation of transmission spectrum (21) for a plate of a 2D resonant photonic crystal of the first type. The crystal consists of infinite nanocomposite cylinders that form a square lattice in vacuum. For silver, $\varepsilon_0 = 5$, $\omega_p = 9$ eV, and $\gamma = 0.02$ eV; for the matrix, $\varepsilon_d = 4.16$. The period of the structure of the photonic crystal is $d = 138$ nm. The filling factor, i.e., the fraction of the nanocomposite in the photonic crystal, is defined by the expression $F = \pi r^2/d^2 = 0.28$, where r is the cylinder radius. The frequency dependences of the real $\varepsilon'_{\mathrm{mix}}(\omega)$ and imaginary $\varepsilon''_{\mathrm{mix}}(\omega)$ parts of the dielectric permittivity that

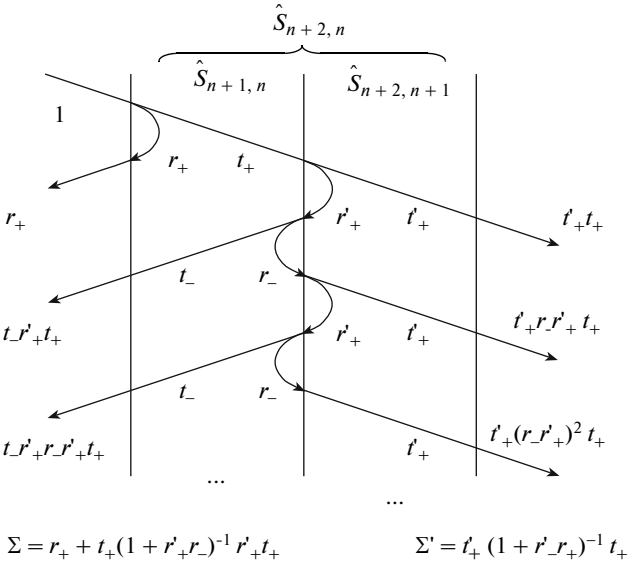

Fig. 3. To the derivation of formula (20) of multiple scattering via the matrix sum of a decreasing geometric progression.

were calculated by formula (1) show that the frequency ω_0 that corresponds to the resonance in cylinders is shifted toward the low-frequency range as the volume concentration of nanospheres increases. In this case, the halfwidth of the resonant curve $\varepsilon''_{\mathrm{mix}}(\omega)$ changes insignificantly, the curve $\varepsilon'_{\mathrm{mix}}(\omega)$ becomes considerably modified, and the frequency range in which $\varepsilon'_{\mathrm{mix}} < 0$ increases. As an example, Fig. 4 shows the dependences $\varepsilon'_{\mathrm{mix}}(\omega)$ and $\varepsilon''_{\mathrm{mix}}(\omega)$ for two values of the filling factor, $f = 0.01$ and $f = 0.1$.

Figure 5a presents a seed transmission spectrum ($f = 0$) for s-polarized waves that propagate in the xy plane along the x axis when the light is normally incident onto the plate from vacuum. The width of the band gap of the transmission spectrum of the plate is consistent with the width of the gap in the x-direction of the Brillouin zone [5] and is in the range from 320 to 473 nm. Figures 5b and 5c show the intensity distribution normalized to the intensity I_0 of the radiation incident onto the sample calculated by formula (22) for the frequency of the first side maximum of the low-frequency boundary of the band gap. It can be seen from these figures that the electromagnetic field is localized at the center of the plate and that sharp intensity maxima of the electromagnetic field that are localized at the centers of rods are observed. If dielectric rods in a 2D photonic crystal are replaced by metallic rods, the effect of localization of the radiation at frequencies that correspond to the boundaries of the band gap is also observed [17].

At a finite concentration of spheres in a nanocomposite, the transmission spectrum qualitatively changes. Thus, at the filling factor $f = 0.01$ and speci-

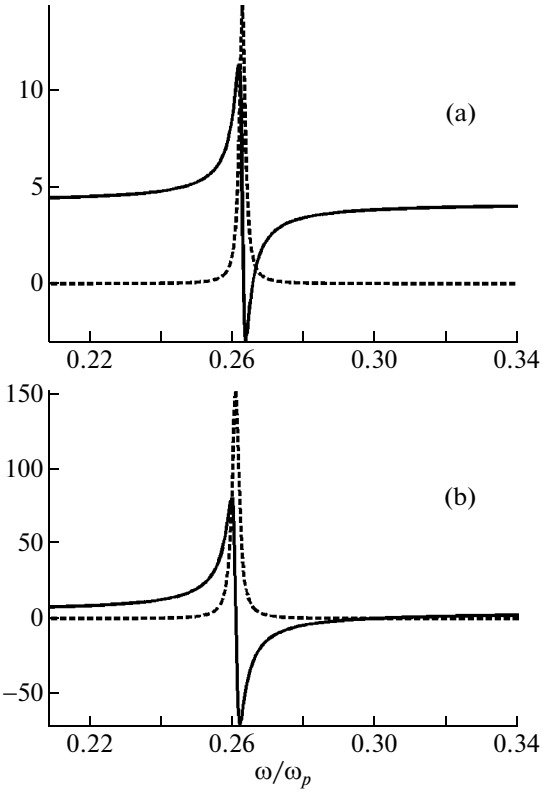

Fig. 4. Dependences of the imaginary (ε''_{mix}, dashed curve) and real (ε'_{mix}, solid curve) parts of the effective dielectric permittivity ε_{mix} on the normalized frequency ω/ω_p. The filling factor is $f =$ (a) 0.01 and (b) 0.1.

fied parameters of the system, the resonant frequency $\omega_0/\omega_p \approx 0.272$ (Fig. 4a) proves to be at the low-frequency edge of the band gap of the seed photonic crystal (Fig. 5a). As a result of the resonant situation that arises in this case, an additional transmission band with a width of ≈25 nm appears in the broadened band gap (Fig. 6a). At a larger factor, $f = 0.1$, and corresponding shift of ω_0 (Fig. 4b), the additional transmission band, as can be seen from the figure, considerably broadens and shifts toward the high-frequency range. As f increases from 0.01 to 0.1, the band gap width increases by 40%. For the frequencies that correspond to the band gap boundaries, the character of the field distribution and the degree of its localization change insignificantly in the cases with $f = 0.01$ and $f = 0.1$. The intensity maxima at the center of the resonant photonic crystal for the frequencies that correspond to the band gap boundaries hardly differ from each other at all at $f = 0.01$ and $f = 0.1$ and are equal to the maximal intensity $I/I_0 = 4$ of the seed photonic crystal (Fig. 5c). However, for the frequencies that correspond to the intensity maxima of additional transmission bands, the intensities at the center of the plate decrease significantly, which is demonstrated in Figs. 6b and 6c.

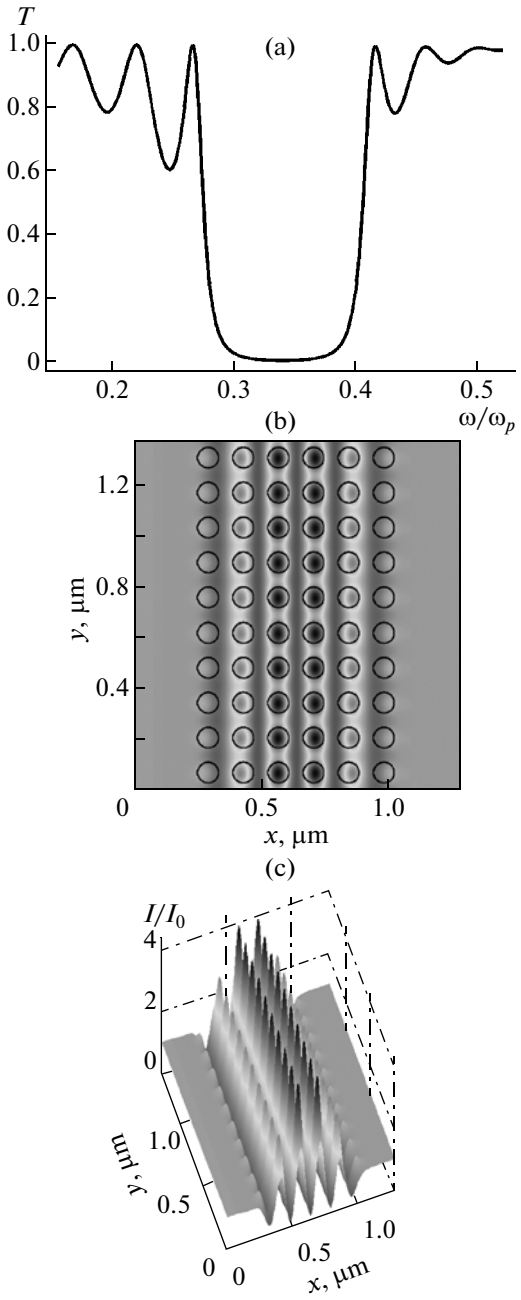

Fig. 5. (a) The transmission coefficient as a function of the frequency for *s* polarized waves that propagate in the plate along the *x*-direction; (b, top view and c, side view) the spatial intensity distribution in a photonic crystal for the frequency of the first side maximum of the low-frequency band gap boundary. The filling factor is $f = 0$.

A characteristic dependence of the transmission spectra on the angle of incidence is presented in Fig. 7 for two crystals of the first type with different lattice constants. For the crystal with the previous period, $d =$ 138 nm, the additional transmission band is shifted with an increase in the angle of incidence. Its width increases with a high-frequency shift of the band gap boundaries in accordance with the Bragg condition

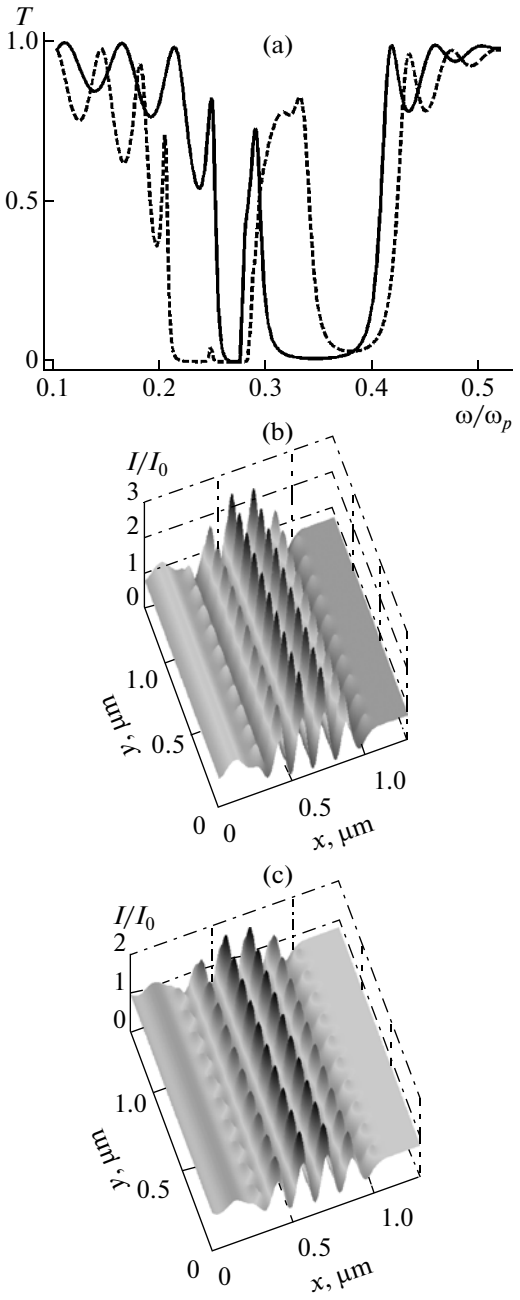

Fig. 6. (a) The frequency dependences of the transmission coefficient calculated for the filling factor $f = 0.01$ (solid curve) and $f = 0.1$ (dashed curve); the angle of incidence is $\theta = 0°$; (b, c) the spatial intensity distributions calculated for the frequency of the maximum of additional transmission in the band gap for the cases $f = 0.01$ and $f = 0.1$, respectively.

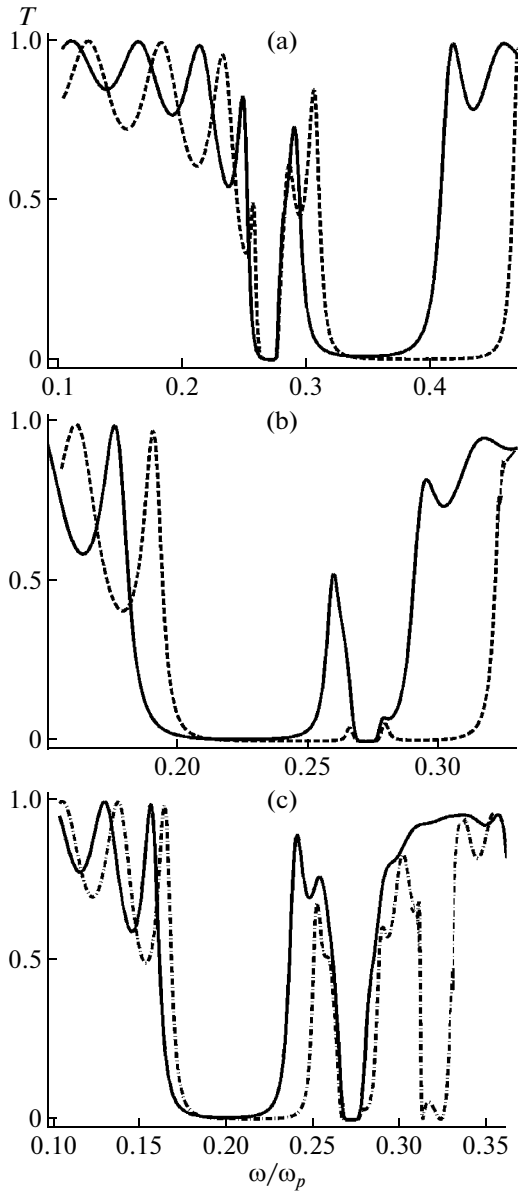

Fig. 7. The frequency dependences of the transmission coefficient at the resonant frequency of resonant photonic crystals with different lattice periods: (a) $d = 138$ nm and $\theta = 0°$ (solid curve) and $\theta = 40°$ (dashed curve), (b) $d_1 = 207$ nm and $\theta = 0°$ (solid curve) and $\theta = 40°$ (dashed curve), and (c) $d_2 = 230$ nm and $\theta = 0°$ (solid curve) and $\theta = 30°$ (dashed-and-dotted curve).

(Fig. 7a). A maximal intensity for the frequency that corresponds to the maximum of the additional transmission curve is observed at the center of the plate. The calculations show that, at $\theta = 40°$, the intensity at the center of the plate is 1.5 times higher compared to the case in which $\theta = 0°$.

An increase in the period to $d_1 = 207$ nm at unchanged factors, $f = 0.01$ and $F = 0.28$, as well as the remaining parameters of the system, leads to a situation that, at $\theta = 0°$, the resonant frequency of the nanocomposite proves to be near the high-frequency boundary of the seed ($f = 0$) band gap. In this case, mixing of photonic modes with the resonant mode causes the band gap to split; as a result of which an additional transmission band appears in the broadened band gap. With increasing θ, the interaction effi-

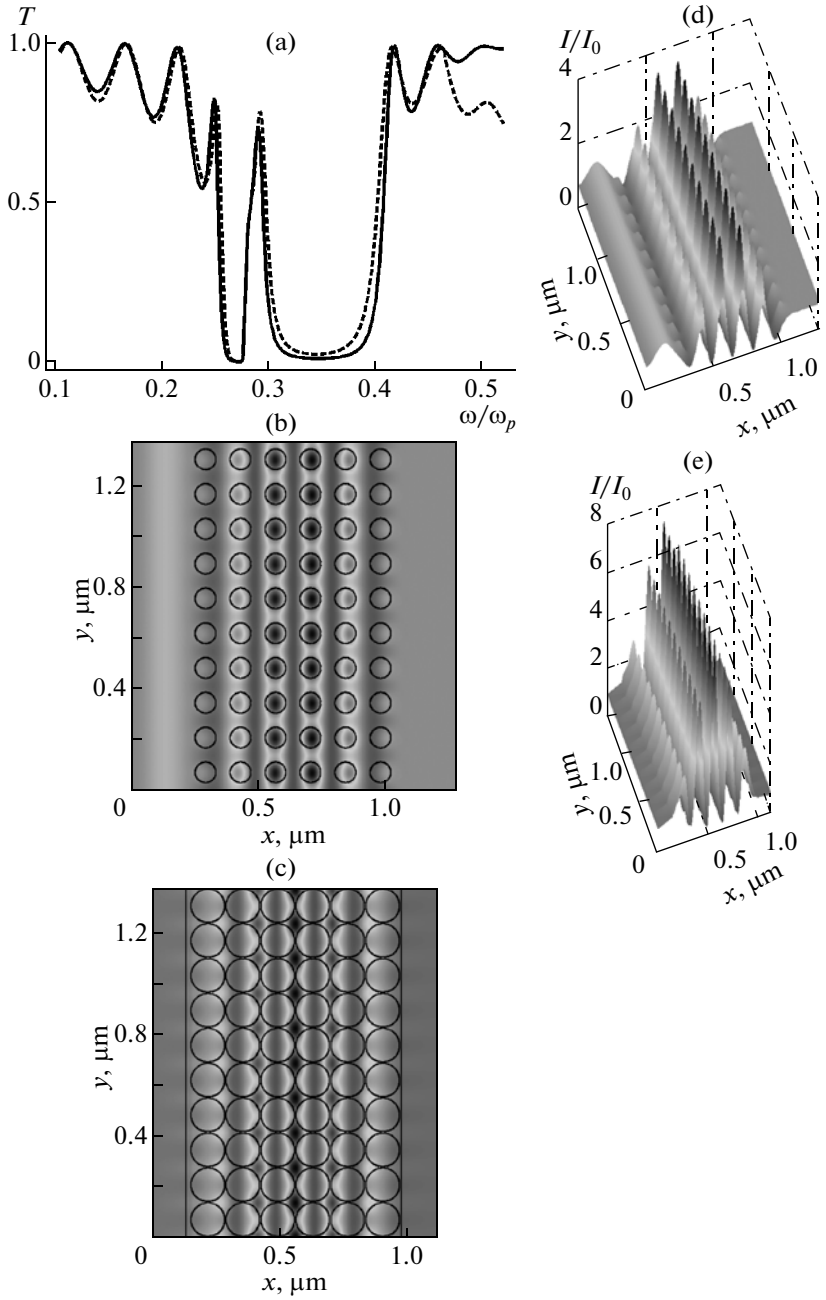

Fig. 8. (a) The frequency dependences of the transmission coefficient calculated for (solid curve) a photonic crystal of the first type with a fraction of nanocomposite $F = 0.28$ and (dashed curve) photonic crystal of the second type with $F = 0.72$. The filling factor is $f = 0.01$. The remaining parameters are the same as in Fig. 6. (b, d, c, e) The intensity distributions for the frequency that corresponds to the low-frequency band gap boundary calculated for (b, top view and d, side view) a photonic crystal of the first type and (c, top view and e, side view) photonic crystal of the second type.

ciency of photonic modes with the resonant mode decreases because the boundary of the seed band gap is shifted toward the high-frequency range. As a result, the additional transmission band almost vanishes and the band gap width increases 1.4-fold (Fig. 7b). A different situation arises if $d_2 = 230$ nm. In this case, the resonant frequency is located in the continuous spectrum of the seed photonic crystal ($f = 0$) and, as a result of mixing of modes, an additional band gap arises (Fig. 7c).

Now, we proceed to consideration of calculation results for the sample of a resonant photonic crystal of the second type, elements of which are empty infinite cylindrical holes that form a square lattice in a nanocomposite matrix. The filling factor is $F = \pi r^2/d^2 = 0.72$. The width of the first band gap of the transmis-

sion spectrum of a plate of a seed photonic crystal ($f = 0$), as in the case of the sample of the crystal of the first type, is consistent with the width of the gap corresponding to the x-direction of the Brillouin zone [5]. For the factor $f = 0.01$, it can be seen from Fig. 8a that, in the range of existence of the band gap of the resonant photonic crystal, the transmission spectra of the crystals of the two types differ insignificantly, which evidently follows from the coincidence of the nanocomposite fractions in the photonic crystals. In addition, the intensity of the electromagnetic field acquires a maximal value at the center of the layer of the resonant photonic crystal and, for the resonant photonic crystal of the second type, it is two times higher than the intensity for the crystal of the first type. Figures 8b, 8d and 8c, 8e show the spatial intensity distribution for the frequency that corresponds to the low-frequency band gap boundary for the crystals of the first (brush) and second (sponge) types, respectively. It can be seen from these figures that the intensity distributions for the resonant photonic crystals of the two types are qualitatively different. Thus, for the crystal of the first type, the localization occurs in nanocomposite rods, whereas, for the crystal of the second type, it is observed in the nanocomposite matrix.

CONCLUSIONS

We calculated the transmission spectra and the spatial intensity distributions for two-dimensional resonant photonic crystals that consist of nanocylinders forming a square lattice in vacuum or, on the contrary, of empty cylinders forming a square lattice in a nanocomposite matrix. We revealed a number of important features in the transmission spectrum of a photonic crystal, which are primarily determined by the resonant character of the effective dielectric permittivity of the nanocomposite and by the significant dependence of this permittivity on the filling factor f, the volume fraction of nanospheres in the dielectric matrix.

We analyzed how the structure of the transmission spectrum and the spatial intensity distribution in 2D resonant photonic crystals vary at different positions of the resonant frequency of the nanocomposite with respect to the boundaries of the seed band gap. We showed that, in the case of equal fractions of the nanocomposite in the photonic crystals, the transmission spectra of the resonant photonic crystals of the two types in the range of existence of the band gap differ insignificantly; however, the spatial intensity distributions have qualitative differences.

The considered effects make it possible to considerably expand the possibilities of controlling the transmission parameters of 2D resonant photonic crystals and the electromagnetic field distribution in the sample by means of variation of the lattice period, the concentration of nanospheres and/or the filling factor of the electromagnetic field of the photonic crystal by the nanocomposite, as well as by means of scanning the band gap with respect to the resonant frequency of the nanocomposite.

ACKNOWLEDGMENTS

This work was supported by grants RNP no. 2.1.1/3455, OFN RAN no. 3.9.1, Presidium of the Russian Academy of Sciences no. 21.1, and "Integration" SO RAN nos. 5 and 144.

REFERENCES

1. J. D. Joannopoulos, R. D. Meade, and J. N. Winn, *Photonic Crystals* (Princeton Univ. Press, Princeton, 1995).
2. K. Sakoda, *Optical Properties of Photonic Crystals*, 2nd ed. (Springer, Berlin, 2004).
3. K. Busch, S. Lolkes, R. B. Wehrspohn, et al., *Photonic Crystals: Advances in Design, Fabrication, and Characterization* (Wiley-VCH, Weinheim, 2004).
4. V. F. Shabanov, S. Ya. Vetrov, and A. V. Shabanov, *Optics of Real Photonic Crystals: Liquid Crystalline Defects and Inhomogeneities* (Izd-vo SO RAN, Novosibirsk, 2005) [in Russian].
5. S. Ya. Vetrov, I. V. Timofeev, and N. V. Rudakova, Phys. Solid State **52** (3), 527 (2010).
6. S. Ya. Vetrov, I. V. Timofeev, and N. V. Rudakova, Phys. Solid State **53** (1), 141 (2011).
7. S. G. Tikhodeev and N. A. Gippius, Usp. Fiz. Nauk **179** (9), 1003 (2009).
8. P. N. Dyachenko and Yu. V. Miklyaev, Optical Memory and Neural Networks (Information Optics) **16** (4), 198 (2007).
9. A. N. Oraevskii and I. E. Protsenko, JETP Lett. **72** (9), 445 (2000).
10. A. N. Oraevskii and I. E. Protsenko, Kvantovaya Elektron. **31** (3), 252 (2001).
11. J. B. Pendry, J. Mod. Opt. **41**, 209 (1994).
12. D. Maystre, Pure Appl. Opt. **3**, 975 (1994).
13. K. S. Yee, IEEE Trans. Anten. Propagat. **14**, 302 (1966).
14. A. Taflove, *Computational Electrodynamics: The Finite-Difference Time-Domain Method* (Artech House, Norwood, 1995).
15. J. C. Maxwell-Garnett, Phil. Trans. Roy. Soc. A **203**, 385 (1904).
16. L. A. Golovan', V. Yu. Timoshenko, and P. K. Kashkarov, Usp. Fiz. Nauk **177** (6), 619 (2007).
17. A. Yu. Vetluzhskii, Tekh. Fiz. Lett. **36** (6), 577 (2010).

Translated by V. Rogovoi